




## Cavity vat photopolymerisation for additive manufacturing of polymer-composite 3D objects

Joel Bachmann <sup>1,2</sup>✉, Philip Obst<sup>2</sup>, Lukas Knorr <sup>2</sup>, Stefan Schmörlzer<sup>3</sup>, Gabriele Fruhmann <sup>2</sup>, Gerd Witt<sup>4</sup>, Tim Osswald<sup>5</sup>, Katrin Wudy<sup>6</sup> & Olaf Hinrichsen<sup>1,7</sup>

Vat photopolymerisation describes resin-based additive manufacturing processes in which ultraviolet light is used to layer-wise solidify liquid resin into a desired 3D shape. If the starting resin is a dual-curing formulation the object is also thermally cured to attain its final properties, obtaining either an elastomer or a thermoset. Here, we introduce cavity vat photopolymerisation, in which one photopolymer resin produces a composite material of an elastomer and thermoset. Cavities of any geometry are purposefully designed in the solid object and then filled with liquid resin during printing due to negative pressure. Thermal curing then solidifies the resin in the cavities into an elastomer, forming a distinct interface held together by strong covalent bonds. Hybrid specimens indicate improved damping, reduced fragmentation upon fracture and increased local elasticity, and we suggest several hard-shell/soft-core applications that might benefit.

<sup>1</sup>Department of Chemistry, Technical University of Munich, Lichtenbergstraße 4, 85748 Garching, Germany. <sup>2</sup>BMW Group FIZ, Knorrstraße 147, 80788 Munich, Germany. <sup>3</sup>NETZSCH-Gerätebau GmbH, Wittelsbacherstraße 42, 95100 Selb, Germany. <sup>4</sup>Department of Engineering, University Duisburg, Lotharstraße 1, 47057 Duisburg, Germany. <sup>5</sup>Polymer Engineering Center, Department of Mechanical Engineering, University of Wisconsin-Madison, Madison, WI 53706, USA. <sup>6</sup>Technical University of Munich, Professorship of Laser-based Additive Manufacturing, Boltzmannstraße 15, 85748 Garching, Germany. <sup>7</sup>Catalysis Research Center, Technical University of Munich, Ernst-Otto-Fischer-Str. 1, 85748 Garching, Germany.

✉email: [joel.bachmann@bmw.de](mailto:joel.bachmann@bmw.de)

Vat photopolymerisation (VPP, official abbreviation according to ISO/ASTM 52900<sup>1</sup>) processes hold the largest material market share in additive manufacturing (AM)<sup>2</sup>. An advantage of resin-based AM approaches is the high accuracy, precision and void-free, completely dense parts with a good surface quality even on the submillimetre scale. Stereolithography (SLA) and digital light processing (DLP) are the best known VPP technologies, but new approaches also have emerged in recent years, such as Digital Light Synthesis (DLS)<sup>3</sup>, volumetric polymerisation inhibition patterning<sup>4</sup> and tomographic volumetric printing<sup>5,6</sup>. In addition, tremendous research efforts are performed on 4D-printing<sup>7,8</sup>, smart materials, and printing materials with hybrid functionalities<sup>9–29</sup>. The big interest in enabling multi-functional materials stems from numerous examples often inspired by nature, such as the resilience in the nacre of the *Pinna nobilis* shell that is achieved by a brick and mortar nanostructure<sup>30</sup>, elastic joints in rigid skeletons that enable flexibility and movement, or other natural products and animals that are tough on the outside though soft on the inside, for example, nuts and crustaceans. From the engineering perspective, qualities like spatially controlled areas with improved shock absorption, crack resistance, damping, elasticity, and hardness are driving the search for AM processes that can produce advanced composites of two different polymer (hard polymer – soft polymer) materials. To create materials designed with spatially different chemical and mechanical properties, one of two approaches is usually followed: either multi-material feedstocks are used in combination with extrusion-based AM<sup>14–22</sup>, Polyjet<sup>24,25</sup>, VPP<sup>11–13</sup> or a combination of different AM processes<sup>23</sup>. Another possibility is that a second orthogonal chemical crosslinking reaction beside the photopolymerisation takes place and creates an interpenetrating network (IPN). The other reaction can be another photopolymerisation, which is initiated by a different wavelength<sup>26,27</sup>; it can also be a catalysed condensation reaction<sup>31</sup> or—as presented in this study—a heat-activated reaction initiated by temperature. However, many approaches to multi-functional, polymer–polymer composites are very difficult to implement because they require additional modifications of existing AM processes, which typically increase the complexity of the already complex process-parameter environment of AM. This makes most of the current approaches slow, expensive and only applicable for minimal build volumes. Moreover, much work needs to be put into the design process, and additional software-specific and process-specific coding is required. For example, Kuang et al.<sup>29</sup> use a code to create a

grayscale distribution that can adjust the modulus of the polymer by generating different light intensities. Finally, one of the biggest challenges in the field of multi-material parts or the composition of two materials is the bonding zone. Typically, this area is the weak point due to material combinations that are chemically often incompatible. In this study, the authors present an AM method called cavity vat photopolymerisation (CVPP), which can produce hard-shell/soft-core polymer composites with a dual-curing resin as a prerequisite. Dual-curing resins are two-part resins that are mixed before printing, UV-cured during vat photopolymerisation and thermally post-cured to attain their final properties. A recent study shows that if the first step of photopolymerisation is omitted and the resin is only thermally cured, this will lead to a fully developed elastomer<sup>32</sup>. The idea behind CVPP is the following: Before printing, cavities are specifically created during the design process in the part where, for example, higher shock absorption or damping is required. Typically, all unvented volumes should be avoided in DLS, as the resin is trapped there by negative pressure. For CVPP, however, the resin inclusion in the cavities serves as an enabler for creating composite 3D objects without any additional processing step. After designing the cavities, CVPP follows the same steps of the dual-curing process known from DLS: printing, post-processing with cleaning, removal of support structures and thermal curing in an oven with a specific temperature profile. In the final post-processing step of thermal curing, the resin is solidified into an elastomer and chemically bonds to the thermoset shell. The application of CVPP does not require any additional processing steps, modification of the process, multi-material feedstock or extra wavelength. It can be broadly applied to all top-down and continuous bottom-up VPP processes (see Fig. 1a). In non-continuous, bottom-up VPP processes that use realignment steps where the part is pulled out of the vat, the resin does not remain in the cavity due to the pressure compensation. However, a modification of CVPP can also be applied for non-continuous, bottom-up VPP by designing inlets to the cavities and injecting dual-curing, liquid resin after the printing process. The sole prerequisite here is the creation of a closed cavity filled with the dual-curing photopolymer resin. For showcasing CVPP, DLS is used as a VPP process, as it provides a continuous bottom-up process and an above-average printing speed through continuous polymerisation, which is enabled by an oxygen-permeable window and a so-called “O<sub>2</sub>-dead zone” (see Fig. 1b). The commercially available and scientifically studied<sup>32–34</sup> DLS material RPU 70 is used as a dual-curing resin formulation. This study

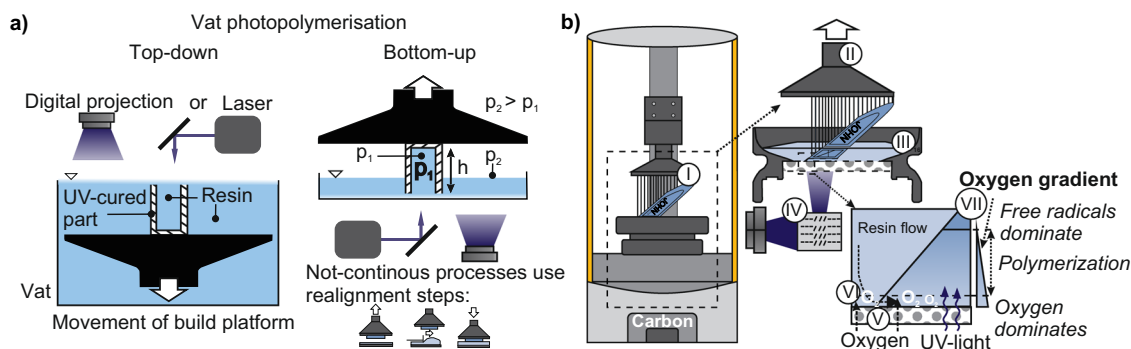


**Fig. 1** Vat photopolymerisation (VPP) technologies suitable for cavity vat photopolymerisation (CVPP). **a** Top-down VPP process, in which resin is solidified on the resin surface and cavities are naturally filled with resin. Bottom-up VPP processes solidify the resin at the bottom of the vat either with UV-laser or digital projection of UV light. Continuous bottom-up VPP processes do not need realignment steps and are suitable for CVPP because cavities are automatically filled with resin because the atmospheric pressure  $p_2$  is greater than the weight pressure  $p_1$  of the resin in the cavity. **b** Graphic depiction of the continuous bottom-up VPP process DLS. (I) Personalised geometry (II) Constant elevation of the build platform (III) Resin-filled vat (IV) DLP system with micro-mirrors (V) Light and oxygen penetrable window (VI) Zone of no polymerisation (VII) UV-cured object.

investigates a print job that is spread over the whole build area to demonstrate that CVPP is simultaneously applied to the entire build area. Even though CVPP can produce complex soft-hard composites in the micrometre range, long uninterrupted and uniform cavities were chosen to demonstrate that the negative pressure keeps the resin in tall geometries (resin-filled cavity height = 15.5 cm in the z-direction) during printing. The scope of this study is to prove that CVPP can take advantage of all benefits of the DLS process like one-step, continuous production of different geometries spread over the build platform and that the resin-filled cavity geometries can be produced with no delay in print time. CT scans and thin-section microscopy of hybrid parts are conducted to investigate the two different phases. To investigate the mechanical and damping properties, tensile, impact testing and dynamic mechanical analysis (DMA) are performed on regular, dense RPU 70 parts (full) and compared to hard-shell/soft-core, thermoset—elastomer parts (hybrid). This study concludes by presenting possible applications of composite 3D objects produced by CVPP.

## Results and discussion

**Printing resin-filled parts and producing hard-shell/soft-core test specimens by CVPP.** Figure 2 shows the printing process steps and specimen produced by the CVPP method. Tensile and impact test specimens from Fig. 2a with a thickness of 4.0 mm were designed as dense parts (series A1–B5) and modified CVPP test specimens with a wall thickness of 1.0 mm (series C1–D5). The specimens were successfully printed (see Fig. 2b), washed and thermally cured. Figure 2c shows a resin-filled impact bar, cut with a scalpel after DLS. The shell releases the enclosed resin. Of course, this step is not the desired result, but it does show that the resin is trapped inside when printing unvented volumes with DLS. The result of CVPP is revealed after thermally curing (see Fig. 2d) the resin-filled specimens. Figure 2e shows the tensile bar C1, cut vertically, revealing its hybrid nature with a hard thermoset shell and a soft elastomer core.

Furthermore, the vertical cross-section of the tensile bar proves that the entire cavity has been filled with resin from top to bottom

during printing. For top-down VPP processes (see Fig. 1a), it seems quite intuitive that liquid resin flows into the cavities. However, for continuous bottom-up processes such as DLS, it seems initially counterintuitive that the resin remains in the cavities, especially when it is drawn out of the vat. Nevertheless, on a second glance, we see this how this principle works in the well-known mercury barometer from Evangelista Torricelli (1608–1647). In his famous experiment, the atmospheric pressure (atm) at sea level keeps mercury in a glass tube at the height of 760 mm (1 atm = 760 mm Hg = 1 torr). The same principle applies to unvented volumes during DLS: the resin in the cavity is exposed only to its own weight pressure  $p_1$ , which is defined by the density of the resin  $\rho_{resin}$  times gravity  $g$  times the height of the uninterrupted resin-filled cavity  $h$ :

$$p_1 = \rho_{resin} \cdot g \cdot h \quad (1)$$

The vat, on the other hand, is exposed to the atmospheric pressure  $p_2$ :

$$p_2 = p_{atm} \quad (2)$$

According to the observation during printing, the resin stays in the cavities, which means:

$$p_1 \leq p_2 \quad (3)$$

$$\rho_{resin} \cdot g \cdot h \leq p_{atm} \quad (4)$$

The hydrostatic pressure would have to overcome the air pressure. Assuming an air pressure of  $p_{atm} = 1013.25$  hPa, the pressure at sea level and the density of the resin used in this study of  $\rho_{resin} = 1010$  kg m<sup>-3</sup>, this leads to:

$$h \leq \frac{p_{atm}}{\rho_{resin} \cdot g} = \frac{101325\text{Pa}}{1010\text{kgm}^{-3} \cdot 9.81\text{ms}^{-2}} = 10.23\text{m} \quad (5)$$

The resin column in the cavity must, therefore, not exceed 10.23 metres. For DLS, the maximum z-direction height for print jobs is

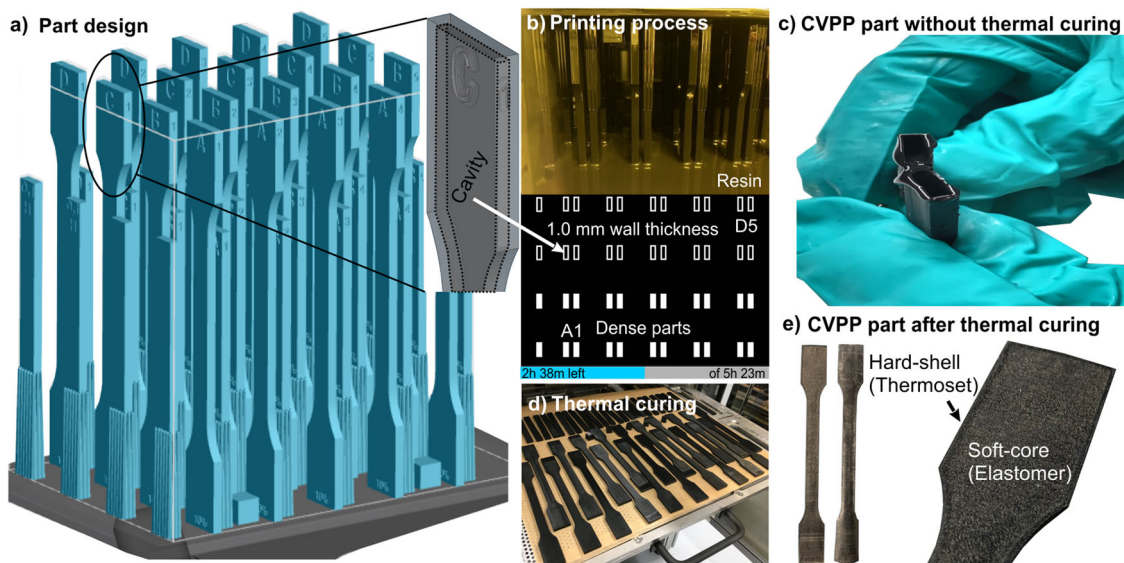


**Fig. 2** Printing resin-filled test specimen and printing hybrid parts via CVPP. **a** DLS print job with 10 full (A1 – B5) and 10 hollow (C1 – D5) tensile (Type A, ISO 3167<sup>40</sup>) and impact specimen (80 × 10 × 4 mm, ISO 179–1eU<sup>36</sup>) on M2 build platform (189 × 118 mm). Maximum z-height of build job = 17.5 cm. Impact specimens are built on support structures to have the testing area at the same height as the tensile test specimen. Magnification shows STL-file of hollow C1 tensile test specimen with a wall thickness of 1.0 mm. **b** Print job during printing (above). Cross-sections of resin-filled and full tensile and impact bars at about 50% (down) **c** Resin-filled impact test specimen after DLS cut open with a scalpel: in cavity trapped liquid resin escapes. **d** Thermal curing of resin-filled and dense UV-cured parts. **e** Hybrid tensile bar (C1) cut vertically in two halves. Magnification shows 1.0 mm wall thickness of thermoset shell and elastomer core.

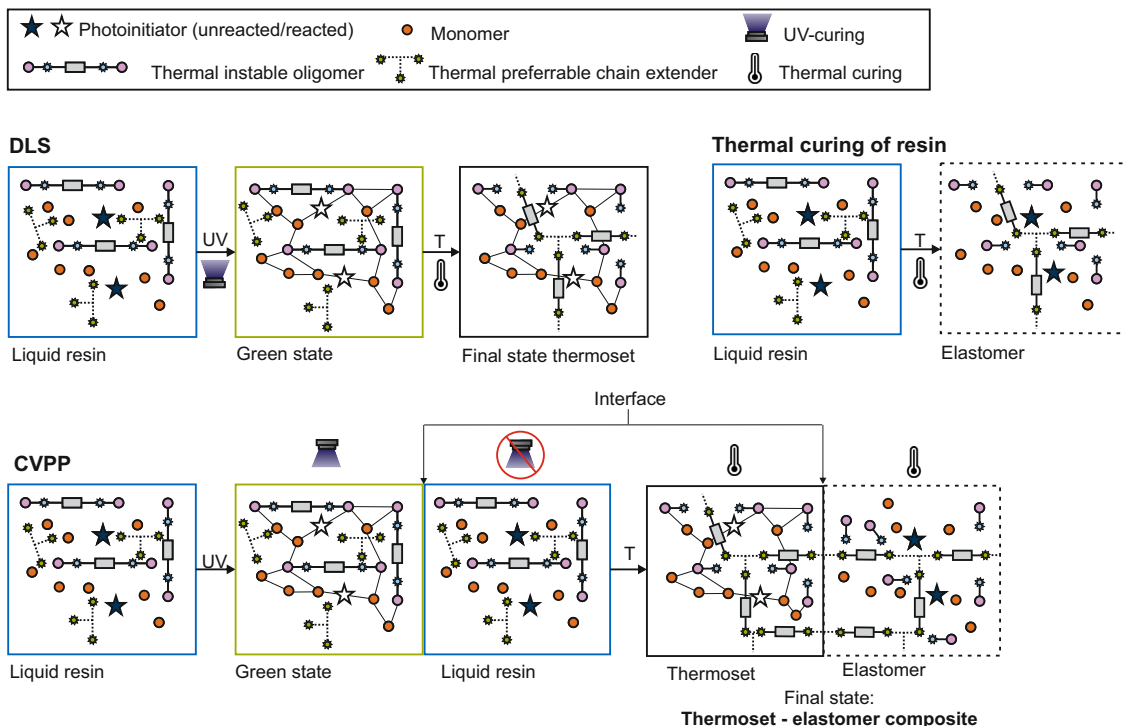


**Fig. 3 Chemistry of dual-curing resin during DLS, purely thermal curing and for CVPP.** The molecules in the liquid resin state (blue square) can move freely. UV light initiates photopolymerization and the first polymer network is formed, also known as the green state (green square). Thermal curing causes the formation of a second polymer network. If the liquid resin is heated, an elastomer (black dashed square) is formed, if the green part is exposed to heat, a thermoset (black square) is formed. The covalent bonds of this second polymer network are the reason for a strong binding strength between the thermoset and elastomer phase in CVPP.

0.46 m, which L1 printers can achieve. Therefore, even for high-density photopolymers, CVPP is not limited by the weight pressure of the resin but by the maximum printing height of conventional printers.

**Dual-curing chemistry as a prerequisite for CVPP.** CVPP requires dual curing, i.e. UV and thermal curing resins. Figure 3 shows a schematic representation of the dual-curing chemistry. The starting material is a liquid resin with photoinitiators, reactive monomers, thermal unstable oligomers and a thermal preferable chain extender. The latter is usually mixed to the reactive composition before printing. To explain the basic principle, the diagram does not include other components such as various monomers, oligomers and passive absorbers. The basic two-step DLS process with UV and thermal curing with the corresponding chemical reactions is shown above. During UV-curing, the photoinitiator triggers photopolymerisation of the reactive (meth-)acrylate groups of the monomers and thermally unstable oligomers. The thermal preferable chain extenders do not take part in this reaction but remain unreacted in the network of the UV-cured (green) state. During the thermal post-process, the “pre-determined breaking points” in the thermally unstable oligomer break up and react with the thermal preferable chain extender. Thermally unstable oligomers combined with thermally preferable chain extenders are the focus of dual-curing resins and the CVPP method. The reaction that occurs can be characterised as a displacement reaction between a strong sterically blocked urethane or urea group. These can be easily synthesised by a sterically hindered (meth-)acrylate like tert-butylaminoethyl methacrylate (TBAEMA) with a diisocyanate. A primary amine

or alcohol can displace TBAEMA from its position and form a thermally stable urea or urethane group, respectively<sup>35</sup>. An in-depth characterisation of the dual-curing chemistry of RPU 70 can be found in the literature<sup>32</sup>, which also refers to the possibility of a thermal reaction of the dual-curing resin to the elastomer. This reaction is also depicted in Fig. 3. CVPP (see Fig. 3 below) combines these two curing chemistries as the body is exposed to UV, but the resin in the cavity is not. In the second step, both the green state body and the resin within are exposed to the thermal curing reaction. Thus, the final state of the outer shell can be characterised as a thermoset with an IPN with the inner core as an elastomer. The thermoset shell is connected to the elastomer core by the thermally preferable chain extender, which is bonded to urea groups in each phase. These strong covalent chemical bonds are unique to CVPP. Other AM, as well as injection-moulding approaches for multi-materials either rely on partial curing, weaker bonds or adhesives. Since CVPP uses the same material for the two different material states, good bonding between them is obvious. FT-IR analysis of the uncured, UV-cured, thermal cured and UV- and thermal cured RPU 70 resin validates the proposed reaction steps (see Fig. 4).

**Non-porous homogeneous phases with a clearly defined interface.** The sharp and strong interface can be best observed in the thin-section microscopy image of a horizontal cross-section of a hybrid tensile bar in Fig. 5a. The density of the final thermoset state ( $\rho_{thermoset} = 1080 \text{ kg m}^{-3}$ ) and the elastomer state ( $\rho_{elastomer} = 1028 \text{ kg m}^{-3}$ ) are very similar, which is reflected in only a low contrast in the CT scan (see Fig. 5b), as this imaging technology relies on density differences. Therefore,

it is well suited to identify remaining air-filled cavities. The horizontal cross-section from Fig. 5b indicates that both phases, namely the thermoset shell and elastomer core, are homogeneous and do not indicate any porosity with enclosed air ( $\rho_{\text{air}} \approx 1.25 \text{ kg m}^{-3}$ ). The Supplementary Movie 1 shows all cross-sections through the 17.5 cm high tensile bar from Fig. 5b: No air bubble can be detected in the entire CT scan. This means that no air is left behind or is dragged into the

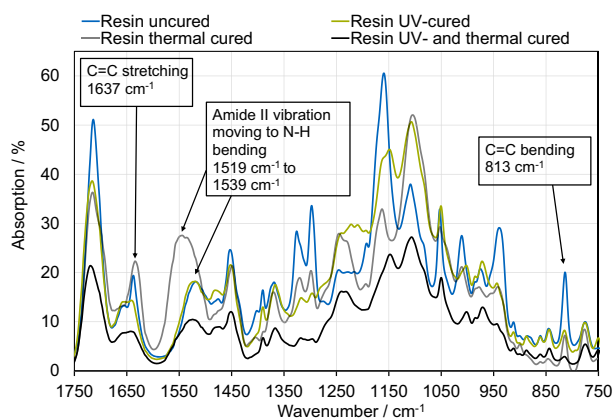


**Fig. 4 FT-IR analysis of RPU 70 resin (resin), UV-cured (green), thermally cured (elastomer) and thermoset (final) state.** The decrease in C=C stretching ( $1637 \text{ cm}^{-1}$ ) and bending ( $813 \text{ cm}^{-1}$ ) signal from resin to green and final state indicates that all photoinitiators and reactive monomers and oligomers have reacted during photopolymerization. The elastomer does not show a decrease in C=C concentration. This means that in the elastomer state, the C=C double bonds have not reacted, and the (meth-)acrylates network is not established. On the other hand, the amide II vibration ( $1519 \text{ cm}^{-1}$ ), which consists of N-H bending and C-N stretching, moves for the elastomer into the N-H bending direction ( $1539 \text{ cm}^{-1}$ ). This behaviour is because the blocking unit (TBAEMA) in the thermally unstable oligomer in the urea group represents a tertiary amine without hydrogen, so no N-H bending is possible. However, the thermal preferable chain extender is a primary amine that replaces the tertiary amine and becomes a secondary amine in the urea group with hydrogen. Therefore, the N-H bending is predominant for the elastomer state and characterizes the thermal reaction.

uninterrupted cavity during printing. Consequently, CVPP can produce two homogeneous, void-free, non-porous phases separated by a well-defined interface.

**Mechanical properties of full and hybrid parts.** Figure 6 shows the results of the mechanical test between the fully dense thermoset (full) and the hard thermoset shell – soft elastomer core hybrid with a 1.0 mm wall thickness (hybrid). At the breaking point, the total material shows brittle fractures with larger and smaller fragments both during tensile (Fig. 6a) and impact testing (Fig. 6b). The hybrid, on the other hand, exhibits an entirely different material behaviour. The elastic core improves elongation at break. At the same time, it reduces tensile strength, impact strength and internal tension before breakage, thereby preventing fragments and even holding the part together after the impact of the pendulum (see Supplementary Movie 2, 3). All mechanical tests were carried out following ISO standards<sup>36–38</sup>. However, these standards are specified for homogeneous parts, something which must be considered when examining and comparing the absolute values between full and hybrid parts summarised in Table 1. The dynamic mechanical analysis (DMA) results displayed in Fig. 6c emphasise the difference in material behaviour between the full and hybrid state. Both the storage ( $E'$ ) and the loss ( $E''$ ) modulus show different curves for the different states.

The hybrid, whose material behaviour is dominated by the elastomer, has a low glass transition temperature ( $T_g$ ) of  $-38 \text{ }^\circ\text{C}$ , typical for elastomers. Below, the  $T_g$ , the material is hard and brittle comparable to glass. Above the  $T_g$  the material demonstrates an elastic or viscoelastic behaviour. The  $T_g$  of the hybrid is a mixed  $T_g$  because the thermoset and elastomer states are compatible. With the ratio of elastomer to thermoset, it is possible to adjust the mixed  $T_g$  and thus also the material behaviour of the hybrid. The full material has a much higher  $T_g$  of  $50 \text{ }^\circ\text{C}$ , and the storage modulus is always above the storage modulus of the hybrid for the entire temperature range. The loss factor  $\tan \delta$ , which represents the damping capacity of the material, is defined as the ratio  $E''/E'$ . The  $\tan \delta$  of the hybrid shows a small shoulder at low temperatures indicating the elastomer and a clear peak at high temperatures, which indicates the thermoset. The elastomer signal in  $\tan \delta$  is less noticeable because the elastomer fraction in the hybrid is smaller than the duromer fraction.

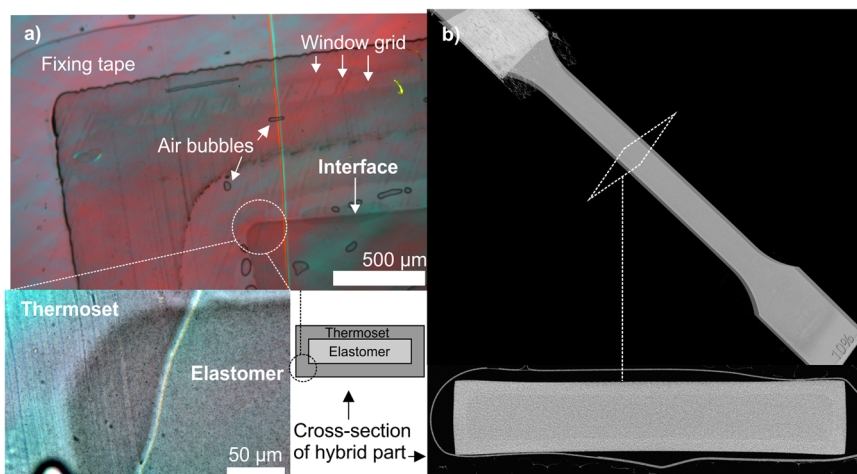


**Fig. 5 Hybrid form part with CT and microscopy analysis.** **a** Cross-section and thin-section microscopy image of hybrid tensile bar. The trapped air bubbles in the image derive from the rough surface, and the fixing tape and are not pores inherent to the two phases. The red line is from the polarisation filter, while the parallel lines in the thermoset phase come from the window grid during DLS. The magnification shows two homogeneous phases with a clearly defined interface between the 1.0 mm thick thermoset shell and the elastomer core. **b** The CT scan of a hybrid C1 tensile bar with 1.0 mm wall thickness and cross-section of CT scan reveals two homogeneous phases without any porosity.

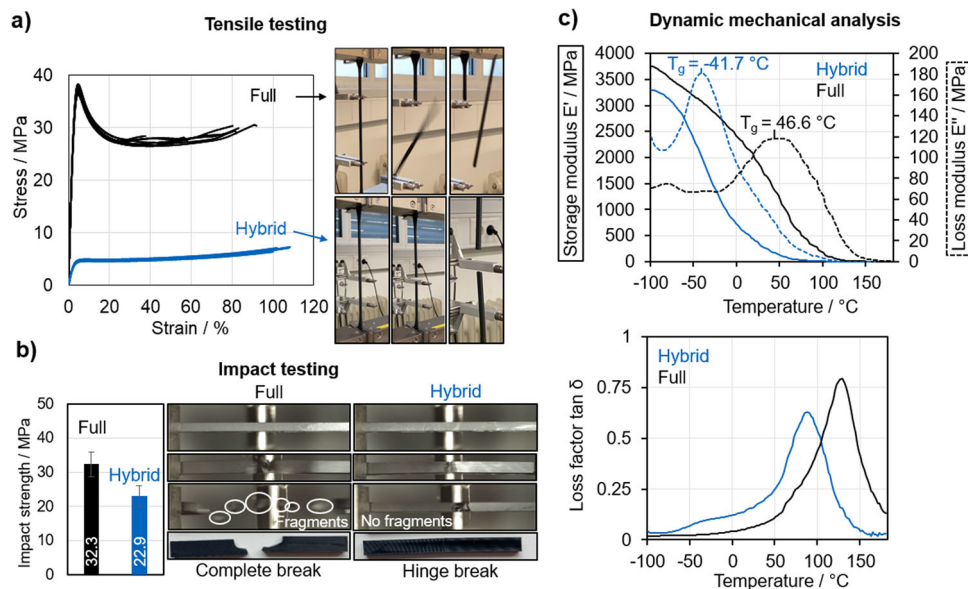


**Fig. 6 Mechanical analysis of thermoset (full) and thermoset - elastomer composite (hybrid) parts.** **a** Tensile testing with images of full and hybrid parts at the breaking point. **b** Impact testing results with SD as error bars. High-speed images at the moment of the pendulum impact and impact bars after testing. **c** DMA measurements. Diagram **c** (on top): — storage modulus - - - loss modulus.

**Table 1 Results of tensile and impact testing without outliers.**

Mechanical Testing		State	N	Mean	Std. Dev.	Minimum	Median	Maximum
Tensile Testing	Cross-section /mm <sup>2</sup>	full	8	38.65	0.13	38.47	38.66	38.81
		hybrid	10	37.00	0.32	36.39	36.94	37.59
	Tensile modulus /MPa	full	8	1300.02	35.14	1248.86	1294.45	1369.37
		hybrid	10	135.54	5.69	122.76	135.49	142.58
	Tensile strength /MPa	full	8	37.42	0.74	36.33	37.52	38.31
		hybrid	10	4.72	0.13	4.53	4.66	4.96
	Elongation at break /%	full	8	71.28	18.48	37.56	80.50	91.99
		hybrid	10	97.30	10.14	78.11	100.75	108.34
Impact Testing	Cross-section /mm <sup>2</sup>	full	10	38.58	0.15	38.33	38.62	38.81
		hybrid	10	40.12	0.16	39.87	40.14	40.36
	Impact strength /MPa	full	10	32.34	3.65	27.15	32.44	38.24
		hybrid	10	22.93	3.22	16.99	22.66	28.71

Furthermore, the hybrid material has superior damping properties up to 100 °C. Therefore, the measurement error, the non-homogeneous sample, is neutralised, and a comparison with the full material is permissible.

**Applications of hybrid materials produced by CVPP.** Engineering demands on automobile wire harnesses are a growing field of AM applications. Parts such as strain reliefs, plugs, grommets and gaiters often have individual geometries that are also size-suitable for AM. The first application from Fig. 7a shows a typical cable strain relief that consists of a robust plug for attaching the part in a bracket. However, to clamp the cable onto the strain relief, the cable holder must be elastic enough to push the cable through. A DLS-printed RPU 70 part does not fulfil the elastic requirement for mounting the cable. However, the hard-shell/soft-core printed part, manufactured by RPU 70 and CVPP, can guarantee both functionalities: the robust plug on the bracket and the elastic cable mounting. The locally designed cavities, with higher elastic requirements in some places, represent the only change from the earlier production. The second example from Fig. 7b is a plug-in, joint-like connector consisting of a plug and a socket. The DLS-printed RPU 70 connector cannot be plugged

into the socket. However, by increasing the elasticity of either the connector or socket locally at the connection point and by designing cavities in the STL file, the plug-in connection works. Both examples demonstrate that not only can uninterrupted, simple geometries be realised, but that complex hybrid geometries can also be produced by CVPP. Of course, it is not only possible to achieve higher elasticity for hybrid parts; locally improved damping and/or fracture behaviour can also be ensured. The latter could be particularly interesting for parts that require high safety standards, such as head impacts, where fragments could become fatal projectiles upon impact. The latter example Fig. 7c shows the infinite possibilities of designing cavities within the part. Small micrometre lattice structures within the part enable different damping properties, moduli and mixed  $T_g$ .

## Conclusion

Several AM attempts have been made to produce parts with hybrid functionalities. However, most approaches call for modification of the AM process, which means that they are not ready for general customer use throughout the AM community. This study presents the method CVPP, which can produce hard-shell/soft-core polymer composites without modifying the DLS

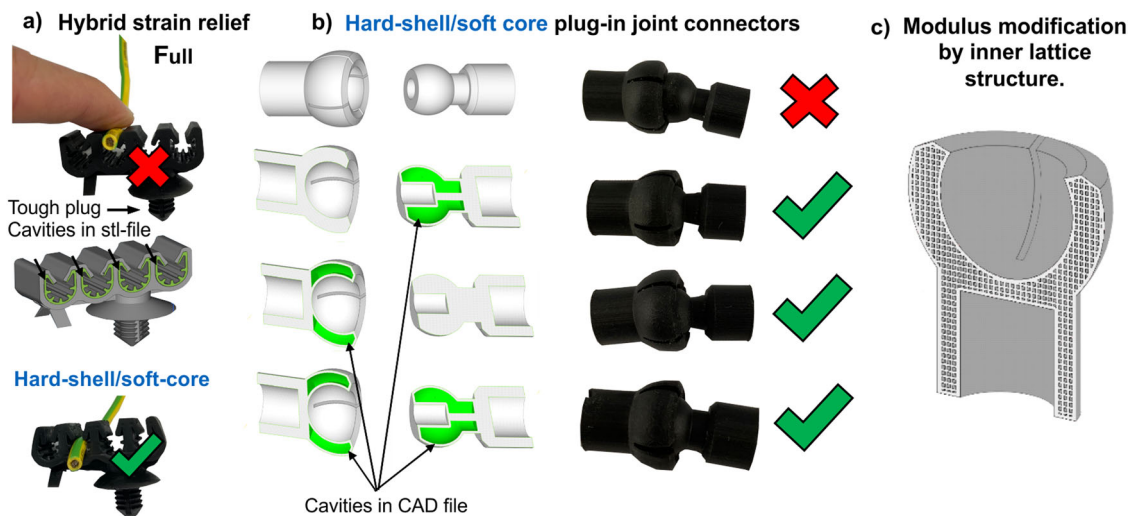


**Fig. 7** Possible applications of hybrid parts produced by CVPP. **a** The hybrid strain relief printed with RPU 70 without modification does not allow to mount a cable. The same part, however, with modified cavities in the area of the desired elasticity allows the fixing of the cable. **b** The Hard shell – soft core connector is another good example of how the design of cavities in the CAD file leads to increased elasticity with CVPP. **c** Inner lattice structures are an outlook on how CVPP could be used to change the modulus of a part.

process. The prerequisites for the implementation of CVPP are threefold:

1. The design of cavities in the CAD file.
2. The use of a dual, i.e. UV and thermal, curing resin like RPU 70.
3. Thermal post processing after the UV-curing step.

The cavities should be designed in areas where the final part requires increased local elasticity, shock absorption and/or damping. Prerequisites here are a dual-curing resin formulation and a thermal post-curing step. CVPP can be broadly applied to all top-down and continuous bottom-up VPP processes (see Fig. 1a). The maximum uninterrupted cavity height is not physically limited and can easily reach the maximum printing height of conventional 3D printers. CVPP can produce two hybrid, homogeneous, non-porous, void-free phases of any geometry with a clearly defined interface. One of the main challenges in the field of multi-material parts is the bonding zone. This is typically the weak point due to chemical, often incompatible material combinations. In this approach, the material is chemically equivalent and, during thermal curing, chemical covalent bonds are formed between the two materials, which provide strong cohesion. The material properties of these hard-shell/soft-core parts can be adjusted between elastomer and thermoset behaviour. Improved fracture behaviour without dangerous projectiles has been demonstrated along with improved damping behaviour at up to 100 °C compared to the full thermoset. The hybrid stress relief part is a perfect example of how CVPP permits hybrid functionalities, starting from one individual photopolymer and by locally designing cavities in the CAD geometry. Several parts in automobile wire harnesses require similar hybrid functionalities. Moreover, the click-and-clip function of joint-like plug-in connectors can be realised by locally increasing the elasticity of the part. It is easy to imagine how CVPP allows endless possibilities of constructing different material properties by varying the amount and size of cavities and elastomeric compartments separated by thermoset lattices. Of course, this can also be applied locally on elements in the part that require a more elastic behaviour or better damping. The thickness of the hard-shell is theoretically limited only by the horizontal resolution of the 3D printer. It should be noted, however, that optimal geometric

designs still need to be found to eliminate sagging and curvatures that may result from the different thermal expansions. Although our approach offers significant benefits, long-term mechanical and chemical stability still needs to be addressed. Furthermore, new dual curing resin formulations will expand the spectrum for even more applications.

## Methods

**Material.** RPU 70 (Carbon, USA) with lot number 20DP2641 was used for all experiments. It consists of two parts: part A and part B, which are mixed in the ratio 10:1 and dispensed at a speed of  $1 \text{ mm s}^{-1}$  into the DLS cassette with an Albion Dispenser (Albion Engineering, USA) before printing. A volume of 460 mL was used for the print job. The volume of the part and support was 287.2 mL. Part A of RPU 70 consists of Diphenyl (2,4,6 trimethyl benzoyl) phosphine oxide (TPO, photoinitiator, 0.1–2%), urethane dimethacrylate (UDMA, difunctional oligomer, 1–20%), methacrylate blocked polyurethane/diisocyanate (MABPU and/or MABDI, blocked prepolymer synthesised with diisocyanates, 10–70%), Isobornyl methacrylate (IBOMA, reactive diluent, 10–50%) and neopentyl glycol dimethacrylate (NPGDMA, difunctional monomer, <0.3%)<sup>39</sup>. Part B of RPU 70 consists of Trimethylolpropane tris [poly (propylene glycol) amine terminated] ether (Chain extender, 20–100%)<sup>39</sup>.

**3D-printing with digital light synthesis (DLS).** The M2 printer (Carbon, USA) with a build volume of  $270 \times 160 \times 380 \text{ mm}$  was used for DLS with a customised print script and build job (see Fig. 2a). The total time for the print was 6 h and 21 min. After the print, the specimens were cleaned in the smart part washer (Carbon, USA) in the default washing mode (7 min) with VF1-Solvent (Vertrel™, MS-767-3D-13). For post-processing, the sample specimens were placed with baking paper on a perforated plate, which was placed in the middle of a Memmert UF 260 TS convection oven (Mettmert GmbH & Co. KG, Germany). The standard thermal curing cycle with a 30 min ramp to 120 °C followed by an isothermal hold for 4 h and then left to cool for to room temperature 30 min.

**Material characterisation.** The weight of the samples was determined by a Cubis® Ultra Micro Balance (Sartorius, Germany). Density measurements of the green and final part were performed by dividing the sample mass by the measured volume of the printed  $10 \times 10 \times 10 \text{ mm}$  cubes. These results were compared with density measurements using the ISO 1183-1 immersion method. Tensile testing was performed with a Type A tensile specimen (ISO 3167<sup>40</sup>) according to ISO 527-1<sup>36</sup> on a Z020 machine (ZwickRoell GmbH & Co. KG, Germany). Impact testing was done on an INSTRON® CEAST 9050 machine (Illinois Tool Works Inc., USA) with a four-joule pendulum and  $10 \times 8 \times 4 \text{ mm}$  unnotched specimen according to ISO 179-1eU<sup>37</sup>. Dynamic mechanical analysis (DMA) was performed on an EPLEXOR® 500 N (NETZSCH-Gerätebau GmbH, Germany) with a  $10 \times 8 \times 4 \text{ mm}$  rectangular specimen in tensile mode according to ISO 6721-1<sup>38</sup>. A measure frequency of 10 Hz, a contact force of 1 N, a static load of 0.3%, a dynamic load of 0.05%, a heating rate of  $2 \text{ K min}^{-1}$  and a temperature range between  $-70 \text{ °C}$  and  $180 \text{ °C}$  was used. The  $T_g$  for the full and hybrid was determined as the peak in the

loss modulus. Fourier transform infrared spectroscopy (FT-IR) was carried out with 16 scans on a mid-infrared ATR unit on a Frontier MIR Spectrometer (PerkinElmer Inc., USA). Eight images were produced via computed tomography (CT) of the hybrid tensile bar C1 using a Phoenix V|tome|x M 240 D | 180 NF Micro-CT machine at a 100 kV voltage, 260  $\mu$ A current, 500 ms exposure time and 20  $\mu$ m isotropic voxel size. A cardboard roll with foam was used to fixate and stabilise the part. Thin-section microscopy images were captured by a PROGRES GRYPHAX<sup>®</sup> NAOS camera (Optische Systeme Jülich GmbH, Germany). A Leica DM LM microscope (Leica Microsystems GmbH, Germany) was used with varying magnifications. To prepare a thin cross-section out of a hybrid impact bar, a rotational HistoCore AUTOCUT automatic microtome (Leica Biosystems Nussloch GmbH, Germany) was used.

Disclaimer for the image integrity: Some images in Figs. 2 and 6 were taken in a laboratory environment with different and sometimes distracting backgrounds. Therefore, the background for these images was cut out.

### Data availability

The data that support the findings of this study are available from the corresponding author upon reasonable request.

Received: 10 June 2021; Accepted: 30 September 2021;

Published online: 26 October 2021

### References

- ISO 52900 (en). *Additive manufacturing — General principles — Terminology*. (2017).
- Wohlers. Wohlers report 2019. 3D printing and additive manufacturing state of the industry (Wohlers Associates, Fort Collins, Colorado, 2019).
- Tumbleston, J. R. et al. Additive manufacturing. Continuous liquid interface production of 3D objects. *Science* **347**, 1349–1352 (2015).
- Beer, M. P. de et al. Rapid, continuous additive manufacturing by volumetric polymerization inhibition patterning. *Sci. Adv.* **5**, eaau8723 (2019).
- Loterie, D., Delrot, P. & Moser, C. High-resolution tomographic volumetric additive manufacturing. *Nat. Commun.* **11**, 852 (2020).
- Bernal, P. N. et al. Volumetric bioprinting of complex living-tissue constructs within seconds. *Adv. Mater.* **31**, e1904209 (2019).
- Kuang, X. et al. Advances in 4D printing: materials and applications. *Adv. Funct. Mater.* **29**, 1805290 (2019).
- Tibbits, S. 4D printing: multi-material shape change. *Archit. Des.* **84**, 116–121 (2014).
- Deore, B. et al. Direct printing of functional 3D objects using polymerization-induced phase separation. *Nat. Commun.* **12**, 55 (2021).
- Huang, J., Ware, H. O. T., Hai, R., Shao, G. & Sun, C. Conformal geometry and multimaterial additive manufacturing through freeform transformation of building layers. *Adv. Mater.* **33**, e2005672 (2021).
- Chen, D. & Zheng, X. Multi-material additive manufacturing of metamaterials with giant, tailorable negative poisson's ratios. *Sci. Rep.* **8**, 9139 (2018).
- Grigoryan, B. et al. Development, characterization, and applications of multi-material stereolithography bioprinting. *Sci. Rep.* **11**, 3171 (2021).
- Hensleigh, R. et al. Charge-programmed three-dimensional printing for multi-material electronic devices. *Nat. Electron.* **3**, 216–224 (2020).
- Podcast: A rapid, multi-material 3D printer, and a bacterium's role in alcoholic hepatitis. *Nature*. <https://doi.org/10.1038/d41586-019-03507-2> (2019).
- Bundell, S. New 3D printer makes multi-material robots. *Nature*. <https://doi.org/10.1038/d41586-019-03513-4> (2019).
- Hardin, J. O., Ober, T. J., Valentine, A. D. & Lewis, J. A. Microfluidic printheads for multimaterial 3D printing of viscoelastic inks. *Adv. Mater.* **27**, 3279–3284 (2015).
- Li, F., Smejkal, P., Macdonald, N. P., Guijt, R. M. & Breadmore, M. C. One-step fabrication of a microfluidic device with an integrated membrane and embedded reagents by multimaterial 3D printing. *Anal. Chem.* **89**, 4701–4707 (2017).
- Loke, G. et al. Structured multimaterial filaments for 3D printing of optoelectronics. *Nat. Commun.* **10**, 4010 (2019).
- Overvelde, J. T. B. How to print multi-material devices in one go. *Nature* **575**, 289–290 (2019).
- Rutz, A. L., Hyland, K. E., Jakus, A. E., Burghardt, W. R. & Shah, R. N. A multimaterial bioink method for 3D printing tunable, cell-compatible hydrogels. *Adv. Mater.* **27**, 1607–1614 (2015).
- Skylar-Scott, M. A., Mueller, J., Visser, C. W. & Lewis, J. A. Voxellated soft matter via multimaterial multinozzle 3D printing. *Nature* **575**, 330–335 (2019).
- Zhou, L.-Y. et al. Multimaterial 3D printing of highly stretchable silicone elastomers. *ACS Appl. Mater. Interfaces* **11**, 23573–23583 (2019).
- Alcántara, C. C. J. et al. Mechanically interlocked 3D multi-material micromachines. *Nat. Commun.* **11**, 5957 (2020).
- Zhang, Y.-F. et al. Fast-response, stiffness-tunable soft actuator by hybrid multimaterial 3D printing. *Adv. Funct. Mater.* **29**, 1806698 (2019).
- Zorzetto, L. et al. Properties and role of interfaces in multimaterial 3D printed composites. *Sci. Rep.* **10**, 22285 (2020).
- Schwartz, J. J. & Boydston, A. J. Multimaterial actinic spatial control 3D and 4D printing. *Nat. Commun.* **10**, 791 (2019).
- Dolinski, N. D. et al. Solution mask liquid lithography (SMaLL) for one-step, multimaterial 3D printing. *Adv. Mater.* **30**, e1800364 (2018).
- Dolinski, N. D. et al. Tough multimaterial interfaces through wavelength-selective 3D printing. *ACS Appl. Mater. Interfaces*. <https://doi.org/10.1021/acscami.1c06062> (2021).
- Kuang, X. et al. Grayscale digital light processing 3D printing for highly functionally graded materials. *Sci. Adv.* **5**, eaav5790 (2019).
- Gim, J. et al. Nanoscale deformation mechanics reveal resilience in nacre of Pinna nobilis shell. *Nat. Commun.* **10**, 4822 (2019).
- Wallin, T. J. et al. 3D printable tough silicone double networks. *Nat. Commun.* **11**, 4000 (2020).
- Bachmann, J. et al. Investigation of the temperature influence on the dual curing urethane-methacrylate resin Rigid Polyurethane 70 (RPU 70) in digital light synthesis (DLS). *Addit. Manuf.* **37**, 101677 (2021).
- Bachmann, J., Gleis, E., Schmöler, S., Fruhmann, G. & Hinrichsen, O. Photo-DSC method for liquid samples used in vat photopolymerization. *Anal. Chim. Acta.* **1153**, 338268 (2021).
- Obst, P. et al. Investigation of the influence of exposure time on the dual-curing reaction of RPU 70 during the DLS process and the resulting mechanical part properties. *Addit. Manuf.* **32**, 101002 (2020).
- Rolland, J. P. et al. *Polyurethane resins having multiple mechanisms of hardening for use in producing three-dimensional objects*. (2015).
- ISO 527-1. *Plastics — Determination of tensile properties* (2019).
- ISO 179-1. *Plastics — Determination of Charpy impact properties* (2010).
- ISO 6721-1. *Plastics — Determination of dynamic mechanical properties* (2019).
- Carbon Inc., Redwood City, CA 94063, USA. SDS Germany RPU 70 Part A and B (2017).
- ISO 3167. *Plastics — Multipurpose test specimens* (2014).

### Acknowledgements

Proofreading was sponsored by the TUM Graduate School and carried out by KERN Corporation. The authors would like to thank Michael Lieberwirth, Stefan Stiel, Stefan Griesing, Johannes Eschl, Gunter Schroeter, Dirk Schuster, Thomas Schromm and Katrin Röckl from the BMW lab for assisting with the mechanical tests, high-speed recordings, CT scans and thin-section microscopy. The authors also thank Rüdiger Selhing from NETZSCH for supporting the DMA measurements.

### Author contributions

J.B.: Conceptualisation, formal analysis, investigation, writing—original draft, writing—review & editing, visualisation, project administration. P.O.: Conceptualisation, Investigation. L.K.: Conceptualisation, Investigation. S.S.: Conceptualisation, Resources. G.F.: Supervision. G.W.: Supervision. T.O.: Supervision. K.W.: Writing—review & editing. O.H.: Writing—review & editing.

### Funding

Open Access funding enabled and organized by Projekt DEAL.

### Competing interests

P.O., L.K. and J.B. are holders of two pending patents related to this work submitted to the German patent and trademark office (Patent 1: Process for additive manufacturing of a form part (DE 10 2020 103 257.9); Patent 2: Production of hard/soft 2 K parts by resin-based additive manufacturing (DE 10 2020 130 690.3)). The other authors declare no competing interests.

### Additional information

**Supplementary information** The online version contains supplementary material available at <https://doi.org/10.1038/s43246-021-00211-5>.

**Correspondence** and requests for materials should be addressed to Joel Bachmann.

**Peer review information** *Communications Materials* thanks the anonymous reviewers for their contribution to the peer review of this work. Primary Handling Editor: John Plummer. Peer reviewer reports are available.

**Reprints and permission information** is available at <http://www.nature.com/reprints>

**Publisher's note** Springer Nature remains neutral with regard to jurisdictional claims in published maps and institutional affiliations.





**Open Access** This article is licensed under a Creative Commons Attribution 4.0 International License, which permits use, sharing, adaptation, distribution and reproduction in any medium or format, as long as you give appropriate credit to the original author(s) and the source, provide a link to the Creative Commons license, and indicate if changes were made. The images or other third party material in this article are included in the article's Creative Commons license, unless indicated otherwise in a credit line to the material. If material is not included in the article's Creative Commons license and your intended use is not permitted by statutory regulation or exceeds the permitted use, you will need to obtain permission directly from the copyright holder. To view a copy of this license, visit <http://creativecommons.org/licenses/by/4.0/>.

© The Author(s) 2021